

Predictions of baryon directed flow in heavy-ion collisions at high baryon density

Yuri B. Ivanov^{1,2,*}

¹*Bogoliubov Laboratory of Theoretical Physics, Joint Institute for Nuclear Research, 141980 Dubna, Russia*
²*National Research Center "Kurchatov Institute", 123182 Moscow, Russia*

Predictions of the proton directed flow (v_1) in semicentral Au+Au collisions in the energy range between 4.5 and 7.7 GeV are done. The calculations are performed within the model of three-fluid dynamics with crossover equation of state, which well reproduces the proton v_1 both below 4.5 GeV and above 7.7 GeV, as well as bulk observables in the energy range of interest. It is predicted that the proton flow evolves non-monotonously. At the energy of 7.2 GeV it exhibits antiproton (i.e. negative slope of $v_1(y)$) in the midrapidity. At 7.7 GeV, the flow returns to the normal pattern in accordance with the STAR data. The midrapidity v_1 -slope excitation functions within the first-order phase and crossover transitions to quark-gluon phase (QGP) turn out to be qualitatively similar, but the amplitude of the wiggle in the crossover scenario is much smaller than that in the strong first-order phase transition. Therefore, the change of sign followed by minimum at 7.2 GeV in the v_1 -slope excitation function indicates onset of (weak phase or crossover) transition to QGP. The second change of the sign around 10 GeV results from interplay between incomplete baryon stopping and transverse expansion of the system.

I. INTRODUCTION

The directed flow is defined as the first coefficient, v_1 , in the Fourier expansion of particle distribution, $d^2N/(dy d\phi)$, in azimuthal angle ϕ with respect to the reaction plane [1, 2]:

$$\frac{d^2N}{dy d\phi} = \frac{dN}{dy} \left(1 + \sum_{n=1}^{\infty} 2 v_n(y) \cos(n\phi) \right), \quad (1)$$

where y is the longitudinal rapidity of a particle. Equation (1) defines so-called transverse-momentum integrated flow coefficients, which are considered below.

The discussion below primarily relates to heavy-ion collisions energies $\sqrt{s_{NN}} = 3$ –12 GeV, at which high baryon density is achieved. This energy range is actively explored in the Beam-Energy Scan (BES) program at RHIC [3] and NA61/SHINE at SPS [4], and will be further studied in forthcoming facilities [5]: NICA [6], FAIR [7], HIAF [8], and J-PARC-HI [9].

The directed flow is one of the most sensitive quantities to the equation of state (EoS) of strongly-interacting matter. Moreover, it provides signals of phase transition to the quark-gluon phase (QGP) [10–15]. However, the directed flow depends not only on the EoS. First of all, it strongly depends on the stopping power of the nuclear matter. The finite stopping power can even mimic the phase transition effect [16]. Though, the stopping power can be constrained proceeding from bulk observables for protons and pions. In Ref. [17], the baryon stopping was even deduced from data on the directed flow. The directed flow of various hadrons is even more involved. In heavy-ion collisions at high baryon density, the directed flow of pions, anti-kaons, Λ s, *etc.* are noticeably modified

during the afterburner stage [18–20], where the nonequilibrium dominates rather than the EoS effects. When the time for the nuclei to pass each other becomes long relative to the characteristic time scale for the participant evolution, the interaction between participants and spectators (so-called shadowing) becomes important [18, 21–23], which strongly modifies the directed flow of various hadrons but not of protons and kaons [18]. The proton flow is only slightly modified by the afterburner and shadowing [18–20] because the baryon matter itself shadows escape of other hadrons. The kaons have a long mean free path and hence are not affected by this shadowing. On the other hand, because of the same long mean free path, the kaons early decouple from the expanding fireball, probably even before the fireball becomes thermalized. Summarizing these arguments, the baryon (proton) directed flow appears to be the most promising observable for studying the EoS effects in heavy-ion collisions at high baryon density.

Data on the directed flow in Au+Au collisions at $\sqrt{s_{NN}} \geq 7.7$ GeV were reported by the STAR collaboration in Ref. [24]. The analysis of these data was performed within various approaches [17, 25–36], which include both hydrodynamic and kinetic models. These studies indicated that the transition to the quark-gluon phase is most probably of the crossover or weak-first-order type [17, 25–27]. It was suggested [17] that the observed sign change in the midrapidity slope of the proton v_1 around 10–20 GeV collision energy is not an evidence of the first-order phase transition of the QCD matter, but rather a consequence of the initial baryon stopping as it was predicted in Ref. [16].

The STAR-FXT (fixed-target) data on the directed flow of identified particles at energies $\sqrt{s_{NN}} = 3$ and 4.5 GeV were recently published in Refs. [37, 38]. These data were also analyzed within various, mostly kinetic models [18, 33, 36, 39–50] in relation to the EoS of the matter produced in these collisions. The kinetic models discussed the directed flow in terms of softness and

*e-mail: yivanov@theor.jinr.ru

stiffness of the EoS [33, 39–41, 43, 46]. They indicated preference of stiff (to a different extent) EoSs for the reproduction of the directed flow at $\sqrt{s_{NN}} = 3$ GeV, while the v_1 data at 4.5 GeV required a softer EoS. The latter was interpreted as indication of onset of transition into QGP. The conclusion about preference of the stiff EoS at 3 GeV contradicts earlier findings. Strong preference of the soft EoS was reported in Refs. [26, 27, 51–53]. In Refs. [26, 27], the EoS is additionally softened at $\sqrt{s_{NN}} > 4$ GeV because of onset of the deconfinement transition. The same conclusion resulted from the analysis of data at 3 and 4.5 GeV within hydrodynamic model [18, 47, 48]. A more extended discussion of the EoS constraints deduced from the directed-flow analysis is presented in review [54].

Very recently, the data on the directed flow (in particular, the proton one) were presented [55] at energies 3.2, 3.5 and 3.9 GeV. These data bridge the STAR results at 3 and 4.5 GeV [37, 38]. However, a very interesting energy range between 4.5 and 7.7 GeV remains experimentally unexplored. Precisely in this energy range, the most spectacular signals of onset of the deconfinement transition are expected.

In this paper the new data on the proton directed flow [55] at energies 3.2, 3.5 and 3.9 GeV are described. Also predictions of the proton directed flow in the energy range between 4.5 and 7.7 GeV are done. The calculations are performed within the model of three-fluid dynamics (3FD) [56, 57]. Different EoSs can be implemented in the 3FD model. Right now, three different EoSs are used in the 3FD simulations: a purely hadronic EoS [58] and two EoSs with deconfinement transitions [59], i.e. an EoS with a first-order phase transition (1PT EoS) and one with a smooth crossover transition. The crossover EoS well reproduces the proton directed flow both below 4.5 GeV and above 7.7 GeV. In addition, it well describes bulk observables [60, 61] in the energy range of interest. Therefore, the crossover predictions for the proton directed flow in the energy range from 4.5 to 7.7 GeV can be considered as reliable. Predictions with two other EoSs are also presented to illustrate sensitivity of the proton directed flow to the EoS.

II. 3FD MODEL AND THESEUS

The 3FD approximation is a minimal way to simulate the early-stage nonequilibrium in the colliding nuclei. The 3FD model [56, 57] describes nonequilibrium at the early stage of nuclear collisions by means of two counterstreaming baryon-rich fluids. In addition, newly produced particles, populating predominantly the midrapidity region, are attributed to a third, so-called fireball fluid. These fluids are governed by conventional hydrodynamic equations coupled by friction terms in the right-hand sides of the Euler equations. The friction terms describe the energy–momentum exchange between the fluids. The 3FD model describes a nuclear collision from the

stage of the incident cold nuclei approaching each other, to the final freeze-out [62, 63]. The freeze-out criterion is $\varepsilon < \varepsilon_{\text{frz}}$, where ε is the total energy density of all three fluids in their common rest frame. The freeze-out energy density $\varepsilon_{\text{frz}} = 0.4$ GeV/fm³ was chosen mostly on the condition of the best reproduction of secondary particle yields for all considered EoSs, see [56].

The 3FD model does not include any kinetic afterburner stage. The THESEUS event generator (Three-fluid Hydrodynamics-based Event Simulator Extended by UrQMD final State interactions) [19, 20, 64], which follows the 3FD simulation, does include the afterburner stage that is described by the UrQMD (Ultrarelativistic Quantum Molecular Dynamics) model [21]. The afterburner stage is of prime importance for collisions at lower energies, where there is no clear rapidity separation between participants and spectators at the freeze-out. When the time for the nuclei to pass each other becomes long relative to the characteristic time scale for the participant evolution, the the expansion of the fireball, consisted of participants, is shadowed by spectators [18, 21–23].

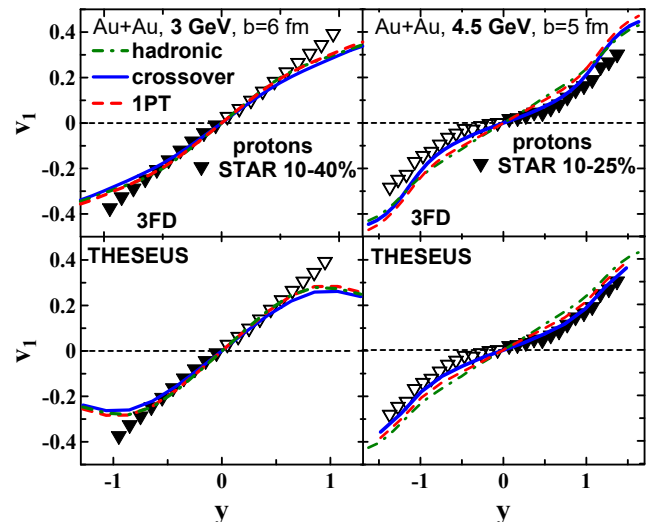


FIG. 1: Directed flow of protons as function of rapidity in semicentral Au+Au collisions at collision energies of $\sqrt{s_{NN}} = 3$ and 4.5 GeV. Results are calculated within the 3FD model (upper row of panels) and the THESEUS [18] (lower row of panels) with hadronic, 1PT, and crossover EoSs. STAR data are from Refs. [37, 38].

Not all observables are equally modified during the afterburner stage. The proton directed flow is only slightly changed [18–20]. This is one of the reasons for choosing the proton v_1 as a preferable observable to quantify the EoS, as it was mentioned in the Introduction. Figure 1 illustrates dependence of the proton v_1 on the afterburner. As seen, the afterburner does not change the proton v_1 in the midrapidity region at 3 GeV and slightly changes at forward/backward rapidities. At 4.5 GeV the proton v_1 is somewhat modified by the afterburner in the midra-

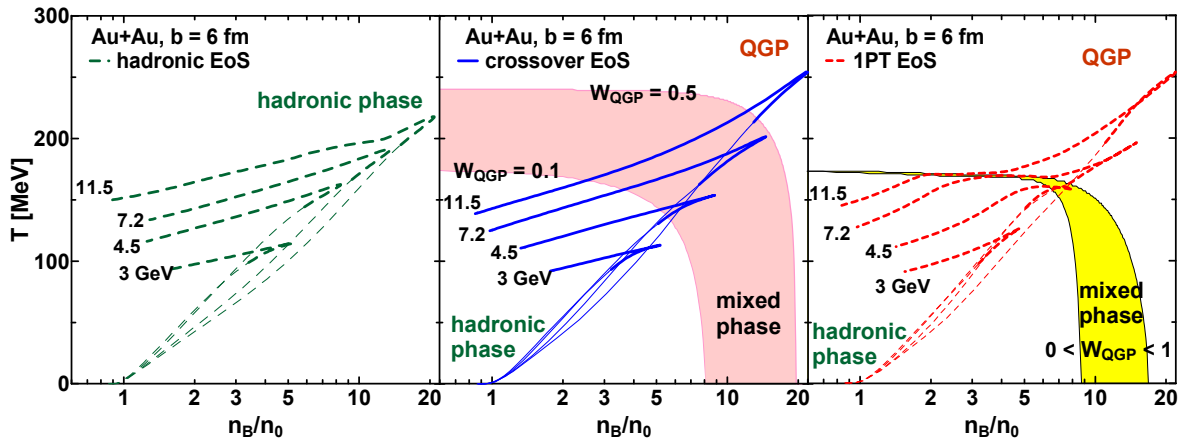


FIG. 2: Dynamical trajectories of the matter in the central cell of the colliding Au+Au nuclei in semicentral collisions (impact parameter is $b = 6$ fm) at energies $\sqrt{s_{NN}} = 3, 4.5, 7.2$ and 11.5 GeV. The trajectories are plotted in terms of the baryon density (n_B , scaled by the normal nuclear density n_0) and temperature T . The trajectories are presented for the three EoSs. The wide shadowed area displays the region of the crossover EoS, where the QGP fraction W_{QGP} lies between 0.1 and 0.5. The shadowed region in the 1PT panel indicates the mixed phase, where $0 < W_{QGP} < 1$.

pidity region making reproduction of the data slightly better. The directed flow of other hadrons is noticeably stronger affected by the afterburner [18–20].

III. EQUATIONS OF STATE

As has been already mentioned, three different EoSs are used in the 3FD simulations: a purely hadronic EoS [58], the EoS with a first-order phase transition (1PT EoS) and one with a smooth crossover transition [59]. The hadronic EoS is quite flexible, it allows for changes of incompressibility. The used version of the hadronic EoS is characterized by incompressibility $K = 190$ MeV. All three EoSs are similar in the hadronic phase. The crossover pressure starts to deviate from the hadronic one at $n_B > 4\text{--}5n_0$ at temperatures 100–150 MeV that are typical for the collisions at STAR-FXT energies, see Fig. 2.

Dynamical trajectories of the matter in the central cell of the colliding Au+Au nuclei in semicentral collisions ($b = 6$ fm) at energies $\sqrt{s_{NN}} = 3, 4.5, 7.2$ and 11.5 GeV are presented in Fig. 2 in terms of the baryon density and temperature. Evolution starts from the normal nuclear density and zero temperature. Thermalization of the matter in this central cell occurs shortly before reaching the turning point, at which density and temperature are maximal [65]. Only after the thermalization the temperature takes its conventional meaning. These thermalized parts of the trajectories are displayed by bold lines. The trajectories for the hadronic and crossover EoSs differ only quantitatively. The 1PT trajectories show also qualitative differences. The 7.2-GeV and 11.5-GeV trajectories exhibit wiggles related to the turn along the mixed-phase region. Even the 4.5-GeV trajectory demonstrates certain flattening after the turning point. This behav-

ior is related to the well-known reheating phenomenon in the first-order phase transition. The temperature along these wiggles does not rise but rather stays nearly constant because the reheating competes with rapid dynamical expansion of the system.

The crossover transition constructed in Ref. [59] is very smooth, it is seen from Fig. 2. Similarly smooth crossover is also implemented in the PHSD model (Parton-Hadron-String Dynamics) [66]. Such a smooth crossover [59] certainly contradicts the lattice QCD data at zero chemical potential [67], which indicate a fast crossover. However, this shortcoming is not severe for the present simulations, in which the system evolves in the region of high baryon densities, where the EoS is not known from the first principles.

When traversing the mixed-phase region of the 1PT EoS, the trajectories pass through the softest-point region, where the isentropic speed of sound (c_s), which is defined as derivative of the pressure (P) over the energy density (ε) at constant entropy (S)

$$c_s^2 = \left(\frac{\partial P}{\partial \varepsilon} \right)_S, \quad (2)$$

exhibits a minimum [10, 13, 14, 68]. At high baryon densities, it is appropriate to speak about the softest-point region rather than the softest point, because the EoS is soft in certain region of temperatures and baryon densities [68]. In the softest-point region, the dynamics of the matter slows down leading to a longer lifetime of the excited system [10]. This results in a significant reduction of transverse expansion (as compared to what it would be without phase transition) and, in particular, to reduction of the directed flow [13, 14]. The softness of the EOS affects not only the transverse, but also the longitudinal expansion. It affects the midrapidity region of the rapidity distribution of net protons in central collisions

and manifests itself as wriggle in the excitation function of the midrapidity curvature of net-proton rapidity distribution [57, 69, 70].

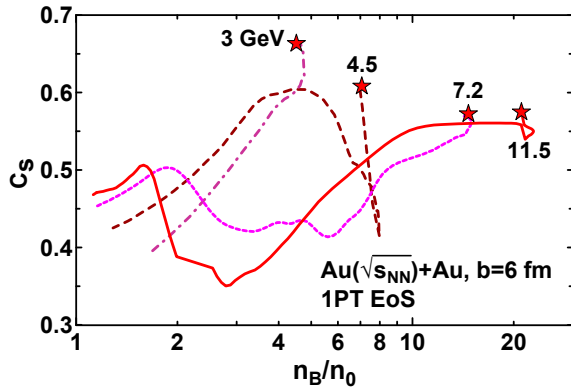


FIG. 3: Evolution of the isentropic speed of sound (c_s) as function of the baryon density (n_B , scaled by the normal nuclear density n_0) along the dynamical trajectories displayed in Fig. 2. The evolution is displayed from the instants (indicated by star symbols) that are close to the trajectory turning points, when the matter is sufficiently thermalized. The trajectories are presented for the 1PT EoS.

The speed of sound along the trajectories (presented in Fig. 2) is displayed in Figs. 3 and 4 for the 1PT and crossover EoSs. The evolution in Figs. 3 and 4 is displayed beginning from instants (indicated by star symbols) when the matter is sufficiently equilibrated [65] and therefore the thermodynamic definition of the speed of sound is appropriate. The equilibration in the central region is attained shortly before reaching the turning point [65], at which density and temperature are maximal, see Fig. 2. After that the evolution of the unified fluid is approximately (up to viscous-like dissipation) isentropic [71] and therefore the speed of sound along the trajectory takes the meaning of the isentropic speed of sound.

As seen from Figs. 2 and 3, the turning point and thus the softest point of the 4.5-GeV trajectory for the 1PT EoS occurs in the mixed phase region. However, this softest-point does not affect the directed flow, as will be seen below, because only the central region of the entire system falls within this softest-point region and only for a short time. The strong effect on v_1 occurs at higher collision energies, when a larger part of the matter falls within this softest-point region and for a longer time. Indeed at energies 7.2 and 11.5 GeV, the trajectories for the 1PT EoS turn out to be captured within the mixed-phase region for some time, see Fig. 2. This results in the softest-point regions in the 7.2-GeV and 11.5-GeV trajectories in Fig. 3.

The c_s evolution for the crossover EoS is quite monotonous except for the cases of the energies of 7.2–11.5 GeV, see Fig. 4. Note that the softest points still exist in the crossover EoS [68], although they are much less pronounced as compared to the 1PT EoS. The crossover 7.2-GeV and 11.5-GeV trajectory exhibit, to different ex-

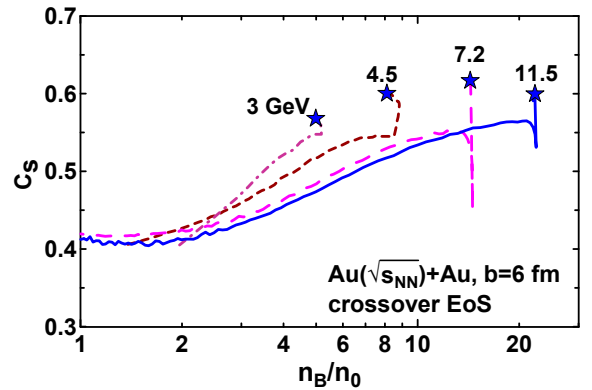


FIG. 4: The same as in Fig. 3 but for the crossover EoS.

tent, behavior similar to that of the 1PT 4.5-GeV one, i.e. exhibit the softest points. This has consequences for the proton v_1 , as it will be seen below.

IV. DIRECTED FLOW

The calculated directed flow of protons as function of rapidity in semicentral Au+Au collisions at collision energies of $\sqrt{s_{NN}} = 3, 3.2, 3.5$ and 3.9 GeV is presented in Fig. 5. These calculations were performed in the 3FD model with hadronic, 1PT, and crossover EoSs. The collision centrality is associated with the corresponding mean impact parameter ($b = 6$ fm) by means of the Glauber simulations based on the nuclear overlap calculator [72], taking into account that colliding nuclei in the 3FD model have the sharp-edge (rather than diffuse edge) density profile. The results are compared with STAR data [38, 55].

As seen, the proton v_1 flow is identical within three considered scenarios at collision energies of 3 and 3.2 GeV. All these scenarios equally well reproduce the experimental data. At 3.5 and 3.9 GeV, the crossover scenario becomes slightly preferable in the midrapidity region. Although its difference from predictions of other scenarios remains insignificant.

Figure 6 demonstrates the flow at collision energies 4.5–11.5 GeV, including predictions for the energies between 4.5 and 7.7 GeV. The directed flow at 5.2–7.2 GeV is calculated for $b = 6$ fm and p_T acceptance of $0.4 < p_T < 2$ GeV/c in order it can be directly compared with results at lower [37, 38, 55] and higher [24] collision energies. Note that the directed flow at 4.5 GeV is also presented for $b = 6$ fm so that it can be compared consistently with v_1 at other energies. While the centrality selection of the data [37] better corresponds to $b = 5$ fm. The Glauber calculator [72] gives the b range between 3.9 and 6.2 fm for the centrality interval 10–25%. We took b just in the middle of this range. This is why the reproduction of the data at 4.5 GeV suffers. If the proper $b = 5$ fm is used as in Fig. 1, the STAR data [37] are better

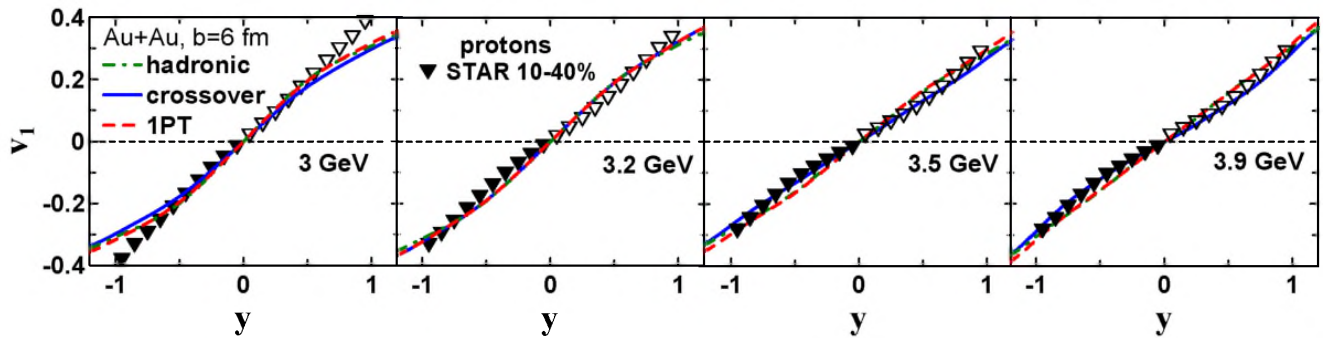


FIG. 5: Directed flow of protons as function of rapidity in semicentral ($b = 6$ fm) Au+Au collisions at collision energies of $\sqrt{s_{NN}} = 3, 3.2, 3.5$ and 3.9 GeV. Results are calculated within the 3FD model with hadronic, 1PT, and crossover EoSs. STAR data are from Refs. [38, 55].

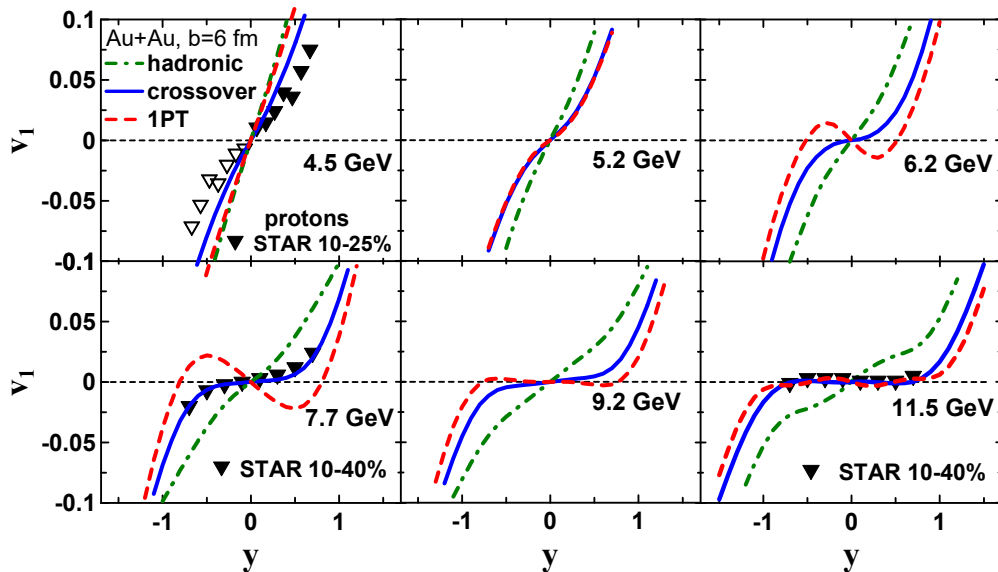


FIG. 6: The same as in Fig. 5 but for collision energies of $\sqrt{s_{NN}} = 4.5, 5.2, 6.2, 7.7,$ and 11.5 GeV. Available STAR data are from Refs. [24, 37].

reproduced within the crossover scenario. At 4.5 GeV, the 1PT proton flow turns out to be almost identical to that for the hadronic EoS, in spite of that the 1PT trajectory touches the mixed phase of the 1PT transition, see Fig. 2. This is because the mixed phase is reached only in the narrow central region of the colliding system and for a short time.

At collision energies above 4.5 GeV, the crossover v_1 becomes distinctly preferable as compared to hadronic and 1PT results. As seen from Fig. 6, the hadronic EoS completely fails to reproduce the available data [24] at 7.7 GeV. The 1PT directed flow behaves precisely as it was predicted in Refs. [13–15]. The proton v_1 first collapses in the midrapidity, then it demonstrates antiflow (i.e. the negative v_1 slope in the midrapidity), after that the flow gradually returns to the normal flow pattern. This antiflow is the effect of the softest-point region that is demonstrated in Fig. 3. It is usually claimed that the

directed flow is formed at the early stage of the collision. This is indeed true for the normal component of the directed flow [14]. Flow and antiflow develop in different rapidity regions [14]. In the early compression stage of the reaction the spectators near projectile and target rapidities are deflected by the pressure in the central hot and dense zone, producing the normal flow. When the expansion of the hot and dense zone proceeds, the antiflow develops around midrapidity. In the course of the expansion, the antiflow occupies a broader region around midrapidity than the normal flow, while the normal flow dominates the region near projectile and target rapidities. When the collision energy increases, the system quickly passes the corresponding softest-point region due to accumulated expansion inertia. Therefore, the influence of that region is essentially reduced. Therefore, the normal flow again becomes dominant in the midrapidity. Thus, the wiggle “flow-antiflow-flow” is a signal of onset

of the phase transition. As seen from Fig. 6, the strong antflow, that is predicted by the 1PT scenario, is not supported by the available data at 7.7 GeV [24].

The crossover v_1 predictions well agree with available data [24, 37]. From the first glance, the midrapidity v_1 slope monotonously decreases between 4.5 and 7.7 GeV. However, a more thorough inspection of this energy region indicates that a weak proton antflow takes place at the energy of 7.2 GeV, see Fig. 7. In order to visual-

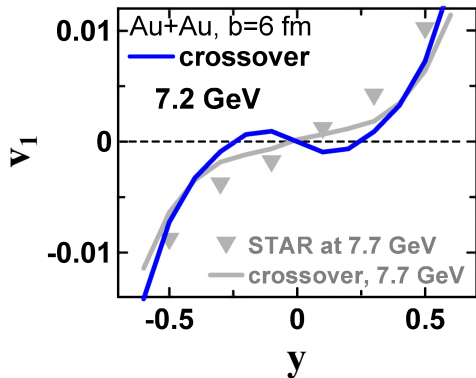


FIG. 7: The same as in Fig. 5 in zoomed midrapidity region but at $\sqrt{s_{NN}} = 7.2$ GeV and only for crossover EoS. STAR data for 7.7 GeV [24] and the corresponding crossover v_1 are also displayed in order to visualize the difference between these energies.

ize the difference between energies 7.2 and 7.7 GeV, the STAR data [24] and the corresponding crossover v_1 at 7.7 GeV are also displayed in Fig. 7. This antflow makes the v_1 evolution with the collision energy rise to be very similar to the case of the 1PT EoS. To see this similarity more clearly, let us consider the excitation function of the midrapidity v_1 slope that is presented in Fig. 8. Both the 1PT and crossover dv_1/dy exhibit dips at 7.2

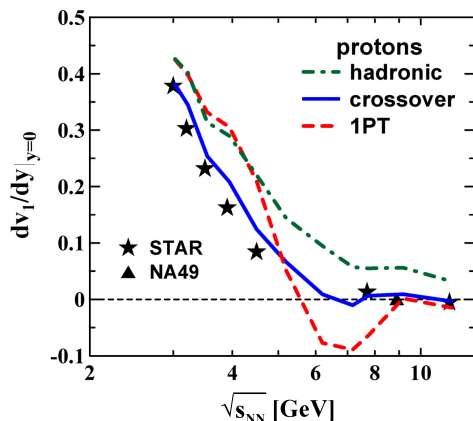


FIG. 8: Midrapidity slope of the proton v_1 as a function of the collision energy $\sqrt{s_{NN}}$ in semicentral Au+Au collisions. Results are calculated within the 3FD model with hadronic, 1PT, and crossover EoS. The data are from Refs. [24, 37, 38, 55] (STAR) and [73] (NA49).

GeV with negative values of the slope then increase to positive values. This is more distinctly seen in Fig. 9, where zoomed energy range of 4–12 GeV is presented.

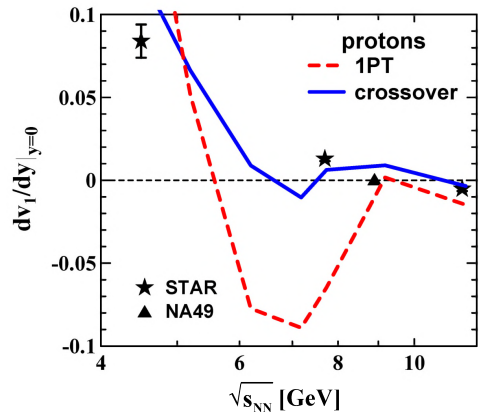


FIG. 9: The same as in Fig. 8 but for the zoomed energy range of 4–12 GeV. The data are from Refs. [24, 37] (STAR) and [73] (NA49).

Figure 9 demonstrates the slope excitation functions within the 1PT and crossover are qualitatively similar, but the amplitude of the wiggle in the crossover scenario is much less than that in the strong first-order transition to QGP (1PT EoS). The first change of sign followed by minimum in the excitation function of the midrapidity slope of the proton v_1 results from onset of (1PT or crossover) transition to QGP. The second change of sign results from correlation of the incomplete baryon stopping and transverse expansion of the system that was predicted in Ref. [16]. This conclusion is confirmed by the fact that both the 1PT and crossover scenarios result in very similar v_1 at collision energies above 9 GeV despite the great difference in the nature of the transition into QGP. This conclusion is also supported by findings in Ref. [17], where it was demonstrated that thorough tune of the baryon stopping allows for good reproduction of the data on the directed flow above 7.7 GeV [24], including the observed change of sign of the proton $dv_1/dy|_{y=0}$ around 10 GeV collision energy. Authors of Ref. [35] also reported that this change of sign around 10 GeV results from interplay between baryon stopping and transverse expansion rather than a phase transition.

The available data on the proton v_1 exclude any strong phase transition while favour a weak phase or crossover transition to QGP. This conclusion that has been already made earlier in Refs. [25–27], agrees with that in Refs. [17, 40].

V. SUMMARY

The directed flow of various particles provides information on dynamics in various parts and at various stages of the colliding system depending on the particle. The

information on the EoS is not always directly accessible because of strong influence of the afterburner stage or insufficient thermalization of the considered probe. The proton directed flow gives the most direct information on the EoS in heavy-ion collisions at high baryon densities because it is minimally affected by the afterburner.

In this paper, new data on the proton directed flow [55] at energies 3.2, 3.5 and 3.9 GeV were considered. Also predictions of the proton directed flow in the energy range between 4.5 and 7.7 GeV were done. Calculations were performed within the 3FD model [56, 57]. The calculations with the crossover EoS [59] well reproduced the proton directed flow [37, 38] at collision energies both below 4.5 GeV [18], including the energies 3.2–3.9 GeV considered in this paper, and above 7.7 GeV [25–27]. In addition, the crossover EoS is favorable for bulk observables [60] in the whole energy range of interest. Therefore, the crossover predictions for the proton directed flow at energies from 4.5 to 7.7 GeV can be considered as reliable predictions. Predictions with two other (hadronic and 1PT) EoSs were also presented to illustrate sensitivity of the proton directed flow to the EoS.

It is predicted that the proton flow evolves non-monotonously in the energy range from 4.5 to 7.7 GeV. At the energy of 7.2 GeV it exhibits antiflow (i.e. negative slope of $v_1(y)$) in the midrapidity. At 7.7 GeV, the flow returns to the normal pattern in accordance with the STAR data [24] and then again exhibits antiflow at

11.5 GeV also in agreement of the STAR data [24].

Thus, the v_1 slope excitation functions within the 1PT and crossover scenarios turned out to be qualitatively similar, but the amplitude of the wiggle in the crossover scenario being much less than that in the strong first-order transition to QGP. The first change of sign followed by minimum in the excitation function of the midrapidity slope of the proton v_1 results from onset of (1PT or crossover) transition to QGP. The second change of sign results from correlation of the incomplete baryon stopping and transverse expansion of the system that was predicted in Ref. [16].

The available data on the proton v_1 exclude any strong phase transition while favour a weak phase or crossover transition to QGP. Experimental observation of the wiggle in excitation function of the midrapidity slope of the proton directed flow at collision energy of 7.2 GeV may confirm this conclusion.

Acknowledgments

Fruitful discussions with D.N. Voskresensky are gratefully acknowledged. This work was carried out using computing resources of the federal collective usage center “Complex for simulation and data processing for mega-science facilities” at NRC “Kurchatov Institute” [74].

-
- [1] S. Voloshin and Y. Zhang, Flow study in relativistic nuclear collisions by Fourier expansion of Azimuthal particle distributions, *Z. Phys. C* **70**, 665 (1996) [arXiv:hep-ph/9407282].
- [2] S. A. Voloshin, A. M. Poskanzer and R. Snellings, in *Relativistic Heavy Ion Physics*, Landolt-Boernstein New Series, I/23, edited by R. Stock (Springer-Verlag, New York, 2010) [arXiv:0809.2949[nucl-ex]].
- [3] A. Aparin [STAR], STAR Experiment Results From Beam Energy Scan Program, *Phys. Atom. Nucl.* **86**, no.5, 758-766 (2023)
- [4] <https://shine.web.cern.ch/>.
- [5] T. Galatyuk, Future facilities for high μ_B physics, *Nucl. Phys. A* **982**, 163-169 (2019)
- [6] <https://nica.jinr.ru/>.
- [7] <https://fair-center.de/>.
- [8] <https://english.imp.cas.cn/research/facilities/HIAF/>.
- [9] <https://asrc.jaea.go.jp/soshiki/gr/hadron/jparc-hi/index.html>.
- [10] C. M. Hung and E. V. Shuryak, “Hydrodynamics near the QCD phase transition: Looking for the longest lived fireball, *Phys. Rev. Lett.* **75**, 4003-4006 (1995) [arXiv:hep-ph/9412360 [hep-ph]].
- [11] D. H. Rischke, Y. Pürsün, J. A. Maruhn, H. Stoecker and W. Greiner, The Phase transition to the quark - gluon plasma and its effects on hydrodynamic flow, *Acta Phys. Hung. A* **1**, 309-322 (1995) [arXiv:nucl-th/9505014 [nucl-th]].
- [12] D. H. Rischke, Hydrodynamics and collective behavior in relativistic nuclear collisions, *Nucl. Phys. A* **610**, 88C-101C (1996) [arXiv:nucl-th/9608024 [nucl-th]].
- [13] L. P. Csernai and D. Rohrlich, *Phys. Lett. B* **458**, 454 (1999) [arXiv:nucl-th/9908034].
- [14] J. Brachmann *et al.* *Phys. Rev. C* **61**, 024909 (2000) [arXiv:nucl-th/9908010].
- [15] H. Stöcker, *Nucl. Phys. A* **750**, 121 (2005) [arXiv:nucl-th/0406018].
- [16] R. J. M. Snellings, H. Sorge, S. A. Voloshin, F. Q. Wang and N. Xu, Novel rapidity dependence of directed flow in high-energy heavy ion collisions, *Phys. Rev. Lett.* **84**, 2803-2805 (2000) [arXiv:nucl-ex/9908001 [nucl-ex]].
- [17] L. Du, C. Shen, S. Jeon and C. Gale, Probing initial baryon stopping and equation of state with rapidity-dependent directed flow of identified particles, *Phys. Rev. C* **108**, no.4, 4 (2023) [arXiv:2211.16408 [nucl-th]].
- [18] Y. B. Ivanov and M. Kozhevnikova, Examination of STAR fixed-target data on directed flow at sNN=3 and 4.5 GeV, *Phys. Rev. C* **110**, no.1, 014907 (2024) [arXiv:2403.02787 [nucl-th]].
- [19] P. Batyuk, D. Blaschke, M. Bleicher, Y. B. Ivanov, I. Karpenko, S. Merts, M. Nahrgang, H. Petersen and O. Rogachevsky, Event simulation based on three-fluid hydrodynamics for collisions at energies available at the Dubna Nuclotron-based Ion Collider Facility and at the Facility for Antiproton and Ion Research in Darmstadt, *Phys. Rev. C* **94**, 044917 (2016) [arXiv:1608.00965 [nucl-th]].
- [20] P. Batyuk, D. Blaschke, M. Bleicher, Y. B. Ivanov,

- I. Karpenko, L. Malinina, S. Merts, M. Nahrgang, H. Petersen and O. Rogachevsky, Three-fluid Hydrodynamics-based Event Simulator Extended by UrQMD final State interactions (THESEUS) for FAIR-NICA-SPSBES/RHIC energies, EPJ Web Conf. **182**, 02056 (2018) [arXiv:1711.07959 [nucl-th]].
- [21] S. A. Bass, C. Hartnack, H. Stoecker and W. Greiner, Out-of-plane pion emission in relativistic heavy ion collisions: Spectroscopy of Delta resonance matter, Phys. Rev. Lett. **71**, 1144-1147 (1993)
- [22] H. Heiselberg and A. M. Levy, Elliptic flow and HBT in noncentral nuclear collisions, Phys. Rev. C **59**, 2716-2727 (1999) [arXiv:nucl-th/9812034 [nucl-th]].
- [23] H. Liu, S. Panitkin and N. Xu, Event anisotropy in high-energy nucleus-nucleus collisions, Phys. Rev. C **59**, 348-353 (1999) [arXiv:nucl-th/9807021 [nucl-th]].
- [24] L. Adamczyk *et al.* [STAR], Beam-Energy Dependence of the Directed Flow of Protons, Antiprotons, and Pions in Au+Au Collisions, Phys. Rev. Lett. **112**, no.16, 162301 (2014) [arXiv:1401.3043 [nucl-ex]].
- [25] V. P. Konchakovski, W. Cassing, Y. B. Ivanov and V. D. Toneev, Examination of the directed flow puzzle in heavy-ion collisions, Phys. Rev. C **90**, no.1, 014903 (2014) [arXiv:1404.2765 [nucl-th]].
- [26] Y. B. Ivanov and A. A. Soldatov, Directed flow indicates a cross-over deconfinement transition in relativistic nuclear collisions, Phys. Rev. C **91**, no.2, 024915 (2015) [arXiv:1412.1669 [nucl-th]].
- [27] Y. B. Ivanov and A. A. Soldatov, What can we learn from the directed flow in heavy-ion collisions at BES RHIC energies?, Eur. Phys. J. A **52**, no.1, 10 (2016) [arXiv:1601.03902 [nucl-th]].
- [28] J. Steinheimer, J. Auvinen, H. Petersen, M. Bleicher and H. Stöcker, Examination of directed flow as a signal for a phase transition in relativistic nuclear collisions, Phys. Rev. C **89**, no.5, 054913 (2014) [arXiv:1402.7236 [nucl-th]].
- [29] Y. Nara, H. Niemi, A. Ohnishi and H. Stöcker, Examination of directed flow as a signature of the softest point of the equation of state in QCD matter, Phys. Rev. C **94**, no.3, 034906 (2016) [arXiv:1601.07692 [hep-ph]].
- [30] C. Shen and S. Alzhrani, Collision-geometry-based 3D initial condition for relativistic heavy-ion collisions, Phys. Rev. C **102**, no.1, 014909 (2020) [arXiv:2003.05852 [nucl-th]].
- [31] S. Ryu, V. Jovic and C. Shen, Probing early-time longitudinal dynamics with the Λ hyperon's spin polarization in relativistic heavy-ion collisions, Phys. Rev. C **104**, no.5, 054908 (2021) [arXiv:2106.08125 [nucl-th]].
- [32] Y. Nara, H. Niemi, J. Steinheimer and H. Stöcker, Equation of state dependence of directed flow in a microscopic transport model, Phys. Lett. B **769**, 543-548 (2017) [arXiv:1611.08023 [nucl-th]].
- [33] Y. Nara, T. Maruyama and H. Stoecker, Momentum-dependent potential and collective flows within the relativistic quantum molecular dynamics approach based on relativistic mean-field theory, Phys. Rev. C **102**, no.2, 024913 (2020) [arXiv:2004.05550 [nucl-th]].
- [34] Y. Nara and H. Stoecker, Sensitivity of the excitation functions of collective flow to relativistic scalar and vector meson interactions in the relativistic quantum molecular dynamics model RQMD.RMF, Phys. Rev. C **100**, no.5, 054902 (2019) [arXiv:1906.03537 [nucl-th]].
- [35] Y. Nara and A. Ohnishi, Mean-field update in the JAM microscopic transport model: Mean-field effects on collective flow in high-energy heavy-ion collisions at $\sqrt{s_{NN}}=2-20$ GeV energies, Phys. Rev. C **105**, no.1, 014911 (2022) [arXiv:2109.07594 [nucl-th]].
- [36] Y. Nara, A. Jinno, K. Murase and A. Ohnishi, Directed flow of Λ in high-energy heavy-ion collisions and Λ potential in dense nuclear matter, Phys. Rev. C **106**, no.4, 044902 (2022) [arXiv:2208.01297 [nucl-th]].
- [37] J. Adam *et al.* [STAR], Flow and interferometry results from Au+Au collisions at $\sqrt{s_{NN}} = 4.5$ GeV, Phys. Rev. C **103**, no.3, 034908 (2021) [arXiv:2007.14005 [nucl-ex]].
- [38] M. S. Abdallah *et al.* [STAR], Disappearance of partonic collectivity in $\sqrt{s_{NN}}=3$ GeV Au+Au collisions at RHIC, Phys. Lett. B **827**, 137003 (2022) [arXiv:2108.00908 [nucl-ex]].
- [39] D. Oliinychenko, A. Sorensen, V. Koch and L. McLerran, Sensitivity of Au+Au collisions to the symmetric nuclear matter equation of state at 2-5 nuclear saturation densities, Phys. Rev. C **108**, no.3, 034908 (2023) [arXiv:2208.11996 [nucl-th]].
- [40] J. Steinheimer, A. Motornenko, A. Sorensen, Y. Nara, V. Koch and M. Bleicher, The high-density equation of state in heavy-ion collisions: constraints from proton flow, Eur. Phys. J. C **82**, no.10, 911 (2022) [arXiv:2208.12091 [nucl-th]].
- [41] M. Omana Kuttan, J. Steinheimer, K. Zhou and H. Stoecker, QCD Equation of State of Dense Nuclear Matter from a Bayesian Analysis of Heavy-Ion Collision Data, Phys. Rev. Lett. **131**, no.20, 202303 (2023) [arXiv:2211.11670 [hep-ph]].
- [42] A. Li, G. C. Yong and Y. X. Zhang, Testing the phase transition parameters inside neutron stars with the production of protons and lambdas in relativistic heavy-ion collisions, Phys. Rev. D **107**, no.4, 043005 (2023) [arXiv:2211.04978 [nucl-th]].
- [43] Z. M. Wu and G. C. Yong, Probing the incompressibility of dense hadronic matter near the QCD phase transition in relativistic heavy-ion collisions, Phys. Rev. C **107**, no.3, 034902 (2023) [arXiv:2302.11065 [nucl-th]].
- [44] P. Parfenov, Model Study of the Energy Dependence of Anisotropic Flow in Heavy-Ion Collisions at $\sqrt{s_{NN}} = 2-4.5$ GeV, Particles **5**, no.4, 561-579 (2022)
- [45] M. Mamaev and A. Taranenko, Toward the System Size Dependence of Anisotropic Flow in Heavy-Ion Collisions at $\sqrt{s_{NN}}=2-5$ GeV, Particles **6**, no.2, 622-637 (2023)
- [46] N. Yao, A. Sorensen, V. Dexheimer and J. Noronha-Hostler, Structure in the speed of sound: from neutron stars to heavy-ion collisions, Phys. Rev. C **109**, no.6, 065803 (2024) doi:10.1103/PhysRevC.109.065803 [arXiv:2311.18819 [nucl-th]].
- [47] M. Kozhevnikova and Y. B. Ivanov, Light-nuclei production in Au+Au collisions at $\sqrt{s_{NN}}=3$ GeV within a thermodynamical approach: Bulk properties and collective flow, Phys. Rev. C **109**, no.1, 014913 (2024) [arXiv:2311.08092 [nucl-th]].
- [48] M. Kozhevnikova and Y. B. Ivanov, Light Hypernuclei Production in Au+Au Collisions at $\sqrt{s_{NN}} = 3$ GeV within Thermodynamic Approach, Phys. Rev. C **109**, no.3, 034901 (2024) [arXiv:2401.04991 [nucl-th]].
- [49] G. C. Yong, Phase diagram determination at fivefold nuclear compression, Phys. Lett. B **848**, 138327 (2024) [arXiv:2306.16005 [nucl-th]].
- [50] S. N. Wei, Z. Q. Feng and W. Z. Jiang, Correlation of the hyperon potential stiffness with hyperon constituents

- in neutron stars and heavy-ion collisions, *Phys. Lett. B* **853**, 138658 (2024) doi:10.1016/j.physletb.2024.138658 [arXiv:2401.07653 [nucl-th]].
- [51] S. Pal, C. M. Ko, Z. w. Lin and B. Zhang, Antiflow of kaons in relativistic heavy ion collisions, *Phys. Rev. C* **62**, 061903 (2000) [arXiv:nucl-th/0009018 [nucl-th]].
- [52] P. Danielewicz, R. Lacey and W. G. Lynch, Determination of the equation of state of dense matter, *Science* **298**, 1592-1596 (2002) [arXiv:nucl-th/0208016 [nucl-th]].
- [53] V. N. Russkikh and Y. B. Ivanov, Collective flow in heavy-ion collisions from AGS to SPS, *Phys. Rev. C* **74**, 034904 (2006) [arXiv:nucl-th/0606007 [nucl-th]].
- [54] A. Sorensen, K. Agarwal, K. W. Brown, Z. Chajecski, P. Danielewicz, C. Drischler, S. Gandolfi, J. W. Holt, M. Kaminski and C. M. Ko, *et al.* Dense nuclear matter equation of state from heavy-ion collisions, *Prog. Part. Nucl. Phys.* **134**, 104080 (2024) [arXiv:2301.13253 [nucl-th]].
- [55] STAR Collaboration, Measurement of Kaon Directed Flow in Au+Au Collisions in the High Baryon Density Region, arXiv:2503.23665 [nucl-ex].
- [56] Y. B. Ivanov, V. N. Russkikh and V. D. Toneev, Relativistic heavy-ion collisions within 3-fluid hydrodynamics: Hadronic scenario, *Phys. Rev. C* **73**, 044904 (2006) [nucl-th/0503088].
- [57] Y. B. Ivanov, Alternative Scenarios of Relativistic Heavy-Ion Collisions: I. Baryon Stopping, *Phys. Rev. C* **87**, no.6, 064904 (2013) [arXiv:1302.5766 [nucl-th]].
- [58] I. N. Mishustin, V. N. Russkikh and L. M. Satarov, Fluid dynamical model of relativistic heavy ion collision, *Sov. J. Nucl. Phys.* **54**, 260-314 (1991).
- [59] A. S. Khvorostukin, V. V. Skokov, V. D. Toneev and K. Redlich, Lattice QCD constraints on the nuclear equation of state, *Eur. Phys. J. C* **48**, 531 (2006) [nucl-th/0605069].
- [60] Y. B. Ivanov, Alternative Scenarios of Relativistic Heavy-Ion Collisions: II. Particle Production, *Phys. Rev. C* **87**, no.6, 064905 (2013) [arXiv:1304.1638 [nucl-th]].
- [61] Y. B. Ivanov and A. A. Soldatov, Bulk Properties of the Matter Produced at Energies of the Beam Energy Scan Program, *Phys. Rev. C* **97**, no.2, 024908 (2018) doi:10.1103/PhysRevC.97.024908 [arXiv:1801.01764 [nucl-th]]. Alternative Scenarios of Relativistic Heavy-Ion Collisions: III. Transverse Momentum Spectra, *Phys. Rev. C* **89**, no.2, 024903 (2014) [arXiv:1311.0109 [nucl-th]].
- [62] V. N. Russkikh and Yu. B. Ivanov, Dynamical freeze-out in 3-fluid hydrodynamics, *Phys. Rev. C* **76**, 054907 (2007) [nucl-th/0611094].
- [63] Yu. B. Ivanov and V. N. Russkikh, On freeze-out problem in relativistic hydrodynamics, *Phys. Atom. Nucl.* **72**, 1238 (2009) [arXiv:0810.2262 [nucl-th]].
- [64] M. Kozhevnikova, Y. B. Ivanov, I. Karpenko, D. Blaschke and O. Rogachevsky, Update of the Three-fluid Hydrodynamics-based Event Simulator: light-nuclei production in heavy-ion collisions, *Phys. Rev. C* **103**, no.4, 044905 (2021) [arXiv:2012.11438 [nucl-th]].
- [65] Y. B. Ivanov and A. A. Soldatov, Equilibration and baryon densities attainable in relativistic heavy-ion collisions, *Phys. Rev. C* **101**, no.2, 024915 (2020) [arXiv:1911.10872 [nucl-th]].
- [66] W. Cassing and E. L. Bratkovskaya, Parton-Hadron-String Dynamics: an off-shell transport approach for relativistic energies, *Nucl. Phys. A* **831**, 215-242 (2009) [arXiv:0907.5331 [nucl-th]].
- [67] Y. Aoki, G. Endrodi, Z. Fodor, S. D. Katz and K. K. Szabo, The Order of the quantum chromodynamics transition predicted by the standard model of particle physics, *Nature* **443**, 675-678 (2006) [arXiv:hep-lat/0611014 [hep-lat]].
- [68] V. D. Toneev, E. G. Nikonov, B. Friman, W. Norenberg and K. Redlich, Strangeness production in nuclear matter and expansion dynamics, *Eur. Phys. J. C* **32**, 399-415 (2003) [arXiv:hep-ph/0308088 [hep-ph]].
- [69] Y. B. Ivanov, Baryon Stopping as a Probe of Deconfinement Onset in Relativistic Heavy-Ion Collisions, *Phys. Lett. B* **721**, 123-130 (2013) [arXiv:1211.2579 [hep-ph]].
- [70] Y. B. Ivanov and D. Blaschke, Robustness of the Baryon-Stopping Signal for the Onset of Deconfinement in Relativistic Heavy-Ion Collisions, *Phys. Rev. C* **92**, no.2, 024916 (2015) [arXiv:1504.03992 [nucl-th]].
- [71] Y. B. Ivanov and A. A. Soldatov, Entropy Production and Effective Viscosity in Heavy-Ion Collisions, *Eur. Phys. J. A* **52**, no.12, 367 (2016) [arXiv:1605.02476 [nucl-th]].
- [72] <http://web-docs.gsi.de/~misko/overlap/interface.html>
- [73] C. Alt et al.(NA49 Collaboration), Directed and elliptic flow of charged pions and protons in Pb+Pb collisions at 40-A-GeV and 158-A-GeV, *Phys. Rev. C* **68**, 034903 (2003) [nucl-ex/0303001].
- [74] <http://ckp.nrcki.ru/>